Hindawi
Shock and Vibration
Volume 2023, Article ID 2400632, 13 pages
https://doi.org/10.1155/2023/2400632

Research Article

Study on Characteristics of Acoustic Emission *b* Value of Coal Rock with Outburst-Proneness under Coupled Static and Dynamic Loads

Kun Zhang, Sen Zhang, Jianxi Ren, Man Wang, Shuai Jing, and Weijun Zhang

School of Architecture and Civil Engineering, Xi'an University of Science and Technology, Xi'an 710054, China

Correspondence should be addressed to Jianxi Ren; renjianxi1968@163.com

Received 10 December 2021; Revised 26 August 2022; Accepted 3 February 2023; Published 17 February 2023

Academic Editor: F. Abio Rizzo

In this paper, a rock dynamic and static triaxial mechanical test system is adopted to conduct triaxial compression failure acoustic emission test on coal rock with outburst-proneness. The purpose is to study the evolution law of the acoustic emission (AE) *b* value of coal rock under static and dynamic load of varying frequencies. The test results show that the dynamic load disturbance will accelerate the instability failure process of coal rock, that the average stress level/ultimate strain of coal rock decline/rises correspondingly with the increasing dynamic load frequency. Moreover, the overall AE *b* value after dynamic load disturbance is relatively low, and the higher the dynamic load frequency, the larger the decrease in the *b* value. In addition, as the dynamic load frequency increases, the AE ringing count and AE energy show a trend of first increasing and then decreasing, and they are negatively correlated with the evolution characteristics of the acoustic emission *b* value. Furthermore, the change rule of AE *b* value is closely related to the instability and failure process of coal rock. A second-stage of the overall *b* value of acoustic emission shows a "cliff jumping type" decrease dip angle or "fault cliff type" decrease dip angle indicates the imminent failure of coal rock, which can be used as an evaluation index for real-time monitoring of dynamic disasters of coal rock with outburst-proneness.

1. Introduction

More than 90% of China's coal is mined underground. Due to the huge demand for coal resources as well as the depletion of shallow resources, deep mining has become the main way of coal mining in China [1]. In deep coal mining, there are high ground stress, high ground temperature, high osmotic pressure, and strong mining disturbance [2]. When the coal of the tunnel is disturbed by the dynamic load caused by construction or geological structure, it is easy to cause instability of the surrounding rock and destruction of the tunnel; in severe cases, rock bursts can be induced, causing great danger to the safety of underground workers and mining construction [3, 4]. There are many problems that need to be addressed in the prevention and control of frequent coal dynamic disasters [5, 6].

Acoustic emission (AE) is a phenomenon in which a local source in a material rapidly releases energy to generate transient elastic waves, also known as stress wave emission [7]. By analyzing the AE signal of the tested material, it is possible to infer the morphological changes inside the material, and to its failure mechanism and damage degree, which is of great positive significance to the prediction of failure and instability of rock engineering. The *b* value law of AE plays an important role in understanding the rock failure mechanism and preventing disaster accidents resulted from rock failure or instability [8].

Liu [9] used fractal theory to study the fractal characteristics of pores of different coal before and after cold leaching in liquid nitrogen and revealed the spatial expansion and connectivity of macroscopic and microscopic pores and fractures in coal during liquid nitrogen fracturing. Based on generalized acoustic emission threshold of rock mass and finite element stress analysis, Cai et al. [10] proposed a new method to calculate rock mass strength parameters from acoustic emission monitoring data. Lou et al.

[11] studied the correlation between acoustic emission, EME and stress drop, and the spectral characteristics of acoustic emission and EME. Manterloa et al. [12] evaluates the fracture toughness of the bonded joint by the acoustic emission test and analyzes the crack propagation characteristics of the bonded joint. Jiang et al. [13] studied the source of acoustic emission signals with different frequencies in tensile fracture, and accurately revealed the instantaneous frequency characteristics of rock tensile fracture failure. Liu et al. [14] used the acoustic emission monitoring system and infrared thermal imager monitoring system to monitor rock burst, revealing the brittle failure characteristics of hard rock exposed by tunnel excavation in humid environment. Schiavi et al. [15] studied the AE during the fracture process of loaded rock mass, and pointed out that the low-frequency AE signals can also be used as the characteristic information of the rock mass failure. Li et al. [16] used Hilbert–Huang transform method to analyze the acoustic emission waveform characteristics, studied the structural damage characteristics of coal rock at different loading stages, and revealed the response law of structural instability and failure evolution of coal rock. Shkuratnik et al. [17] studied the acoustic emission characteristics of coal under different stress paths, and analyzed the correlation between acoustic emission and internal structure of rock samples. Scholars have studied the macroscopic and microscopic crack propagation law and acoustic emission evolution characteristics of rock failure under static load, but the acoustic emission evolution characteristics of rock failure under dynamic load are not given.

Liu et al. [18] carried out the fatigue mechanical property test of the synthetic jointed rock model under four loading frequencies, four maximum stresses and four amplitudes, and revealed the influence of the cyclic loading parameters on the mechanical properties of the jointed rock model. Feng et al. [19] studied the fracture morphology of coal under dynamic impact load based on the multifractal method, proposed the multifractal spectrum parameters to describe the fracture morphology of coal, and found that the fracture surface of coal under dynamic impact load had an obvious anisotropic effect. Lai et al. [20] conducted a numerical simulation test on the full mining stage of the mining face, and studied the mechanism of coal pillar rock burst in the overlying coal body area. Li et al. [21] studied the relationship between energy accumulation and dissipation in the process of dynamic deformation and fracture of coal rock, obtained the energy conditions of rock burst and revealed the evolution process of rock burst. Kong et al. [22] analyzed the influence of axial static load, confining pressure, gas pressure, and impact load on the dynamic mechanical properties of coal samples. Lai et al. [23] conducted impact tests to analyze the damage evolution characteristics of coal under impact loads. Dai et al. [24] carried out the acoustic emission test on the Brazilian disc specimen with herringbone notch, and analyzed the correlation between the dynamic fracture toughness of rock and its cracking section. Sun et al. [25] revealed the relationship between coal rock stress and acoustic emission under multistage dynamic loading. Scholars have studied the mechanical properties and acoustic emission characteristics of unstable failure of hard rock or soft rock/coal under dynamic loading, but there are still insufficient studies on the evolution law of acoustic emission of unstable failure under the dynamic and static combined loading of rock/coal actual occurrence environment.

Zhou et al. [26] carried out the axial static prestress impact test on sandstone and analyzed the failure characteristics of rocks under the actual engineering conditions of static geostress and dynamic disturbance. Xu et al. [27] studied the compression-shear characteristics and failure mechanism of inclined cylindrical rock samples under combined dynamic and static loads. Yan et al. [28] studied the effects of precompression and strain rate on dynamic strength and cracking behavior of single disturbed rock samples by static-dynamic coupling loading test. Yan et al. [29] carried out static-dynamic coupling compression tests on multidefect rock samples. The effects of prestress ratio, crack dip angle, and strain rate on dynamic progressive cracking mechanism and energy evolution of multicrack rock were studied. Li et al. [30] studied the physical stress state of siltstone samples under static and dynamic stress coupling. Weng et al. [31] carried out monotonic axial and static combined loading tests on rock samples with microtunnels to analyze the stability of underground caverns under high geostress conditions. Li et al. [32] reveals the failure mechanism of rock mass with composite cracks under dynamic-static coupling load. Yang et al. [33] used the triaxial compression dynamic-static test system to perform comparative tests on the characteristics of mechanics, permeability, wave velocity, and AE of granite before and after one-dimensional dynamic and static combined loading, and obtained the evolution law of the mechanical properties of deep engineering rock masses under dynamic load disturbance. Zhao et al. [34] carried out the crushing test of granite under dynamic and static combined loading, and found the relationship between total acoustic emission energy and crushing volume under different loading modes and rock breaking effect. Scholars have studied the mechanical properties and acoustic emission characteristics of hard rock under static and dynamic combined loading, but the research on crack propagation and acoustic emission evolution characteristics of soft rocks under static and dynamic combined loading is still insufficient.

In order to explore the premonitory information of rock failure under different confining pressures, Zhang et al. [35] carried out a conventional triaxial loading failure test on marble samples, and analyzed the variation characteristics of AE and its frequency and b value at each stage of marble deformation and failure. Mogi [36] found through experiments that the AE b value of rocks can reflect the inhomogeneity inside the rock. Lei [37] conducted rock tests, and pointed out that the AE b value will decrease systematically before rock failure. Tang et al. [38] based on acoustic emission ring number and b value, using digital image correlation and acoustic emission technology, the fracture test of the three-point bending notched granite beam under cyclic loading was carried out, and the damage evolution process of the sample under cyclic loading was analyzed. Liu

et al. [39] carried out AE tests on granite specimens, respectively, under impact loading and uniaxial compression at different loading rates, and revealed the b value characteristics of AE for rock fracture under various loading conditions. Sagar et al. [40] studied the fracture process of concrete and mortar specimens by testing notched three-point bending specimens, and analyzed the acoustic emission b value characteristics of plain concrete and cement mortar during loading. Calabrese et al. [41] studied the hydrogen induced cracking of martensitic stainless steel in the thiosulfate solution based on acoustic emission mode time evolution analysis, and analyzed the correlation between acoustic emission b value and acoustic event energy time domain distribution. Goebel et al. [42] studied the variation characteristics of seismic b value of acoustic emission events during stress accumulation and release in the laboratory-made fault zone, and analyzed the correlation between acoustic emission b value cycle and periodic stress change. Niu et al. [43] carried out the uniaxial compression test on fractured red sandstone samples, and accurately predicted large-scale events in the fracture process of fractured rocks based on the b value of acoustic emission parameters. Through the true triaxial compression test of granite specimens, Dong et al. [44] analyzed the b value characteristics of acoustic emission events, and supplemented the useful information to distinguish the precursor of rock mass instability. Scholars have revealed the evolution characteristics of acoustic emission b value during the failure process of hard rocks and the application of acoustic emission b value in different research fields. As a kind of semihard brittle rock with multiple fissures, coal belongs to anisotropic nonuniform medium, which is different from the rock in physical and mechanical properties. However, what are the differences in the evolution characteristics of acoustic emission b value of coal and rock participating in failure under dynamic load, and how it differs from the impact-prone coal is still unknown.

With the increase of mining depth, the static load of deep coal rock mass has gradually increased by in situ stress and tectonic stress, and the occurrence conditions of coal seam stress are more complex. When subjected to dynamic loads such as roof fracture, fault sliding, artificial blasting, mining disturbance, or natural earthquake, it may cause major rock burst and other dynamic disasters [45–48]. In carrying out the dynamic load simulation test of coal rock mass, the whole process of coal rock mass failure should be analyzed in detail and quantitatively according to the scientific attitude of combining macro and micro, so as to systematically analyze and describe the whole process and essence of coal rock mass failure.

To sum up, scholars have expanded the approach to study the dynamic damage of coal rock by using acoustic emission. But mostly hard rock, nonimpact tendency coal rock as the main research object, the research on acoustic emission b value characteristics of impact-prone coal rock which are damaged under dynamic loads is still insufficient. Thus, based on previous studies, this paper uses a self-developed rock high-pressure dynamic-static three-axis mechanical test system, combine with the American PAC digital acoustic emission detection system, to carry out a dynamic and static load test on coal rock in deep mine. Through the triaxial compression failure AE test on coal rock under different loading frequencies, the failure law of the coal rock under coupled static and dynamic loads and the evolution characteristics of the corresponding AE b value are discussed. It is expected to provide new ideas for the research on the prediction and prevention of deep coal rock dynamic disasters.

2. Physical Meaning and Calculation of AE b Value

2.1. Physical Meaning of AE. Acoustic emission is the acoustic wave phenomenon monitored by strain energy release in the process of coal rock deformation and failure. Acoustic emission events can be considered as a microseismic activity. Acoustic emission b value is a parameter characterizing the magnitude-frequency relationship of earthquakes, and its physical significance is the measurement of crack development and change. The evolution law of acoustic emission b value in the process of coal rock deformation and failure is studied, and the variation characteristics of the coal rock from crack and crack extension to overall instability failure are revealed. It has important guiding significance for analyzing coal rock failure mechanism and preventing disaster accidents caused by coal rock failure and instability [49].

2.2. Calculation of AE b Value. In 1941, the G-R relationship between earthquake magnitude and frequency was first proposed by Gutenberg and Richter [50] when studying world seismicity:

$$\lg N = a - bM. \tag{1}$$

In the formula, M-earthquake magnitude; N-the earthquake frequency in the range of $M + \Delta M$; a, b-constant.

When calculating the AE b value in the process of coal rock failure, the amplitude of AE is generally used to reflect the magnitude of the AE event because there is no concept of magnitude in AE monitoring. The acoustic emission amplitude (dB) monitored during the test is divided by 20 to obtain the equivalent earthquake magnitude, so that the distribution of the acoustic emission amplitude catalogue and the earthquake magnitude catalogue are roughly consistent [51]. The Gutenberg– Ritcher formula is revised as follows:

$$\lg(N) = a - b\frac{A_{dB}}{20}, \qquad A_{\mathrm{dB}} = 10\lg A_{\max}^2 = 20\lg A_{\max}. \tag{2}$$

Since the least squares method uses a visible straight line to fit the existing cumulative amplitude distribution scatter plot, the obtained results are more intuitive [52]. Thus, this paper uses the least squares method to calculate the AE b value. The formula for calculating the AE b value of coal rock failure by the least square method is revised as follows [53]:

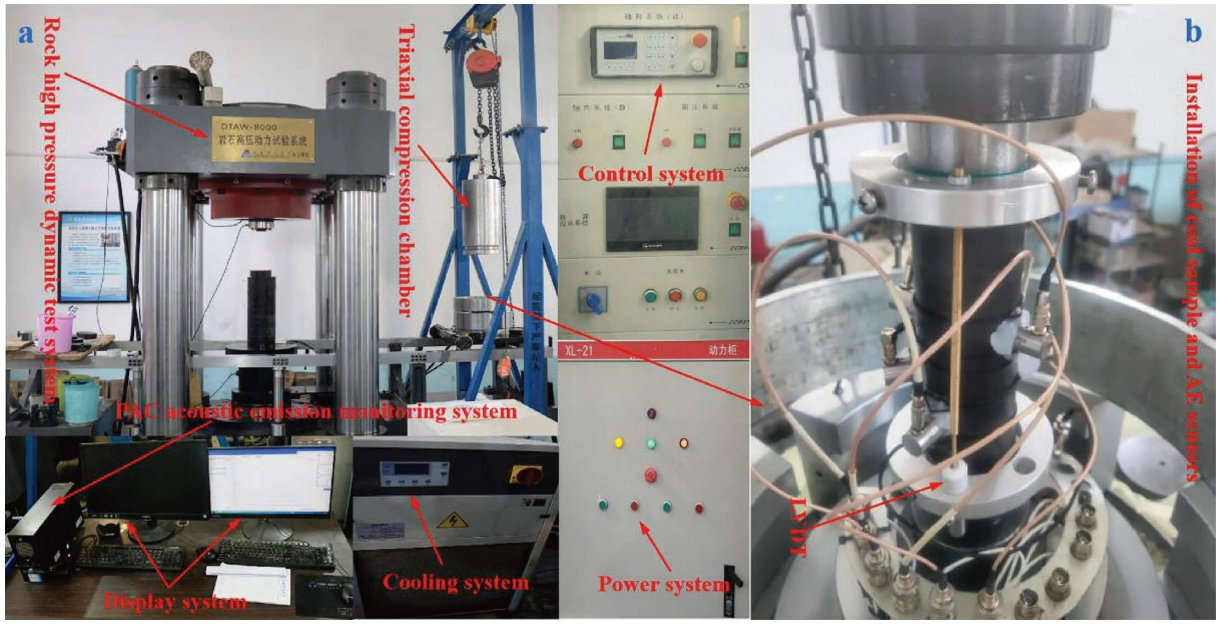

Figure 1: (a) Static-dynamic triaxial mechanical and acoustic characteristics test system; (b) installation of the coal sample and AE sensors.

$$\lg\left[N\left(\frac{A_{dB}}{20}\right)\right] = a - b \times \left(\frac{A_{dB}}{20}\right). \tag{3}$$

In the formula, A_{dB}-acoustic emission event amplitude in decibels; A_{max}-maximum amplitude of the acoustic emission event in microvolts; $N(A_{dB}/20)$-the cumulative number of acoustic emission events with an amplitude $\geq A_{dB}/20$; a -empirical constant, reflecting seismic activity; b-the b value of acoustic emission, reflecting the proportional relationship between large and small earthquakes. AE b value is not only a functional value of AE relative to the magnitude distribution, but also a function that characterizes the expansion scale of cracks inside the coal rock. Its overall magnitude and change trend vary with the development of cracks inside the coal rock.

3. Test Design and Methods

3.1. Test System. The dynamic-static triaxial loading system for mechanical characteristics test of deep rock was used for the static and dynamic triaxial loading of the coal rock. This system consists of a rock high-pressure dynamic test system, a control system, a display system, a PAC acoustic emission detection system, and a cooling system (Figure 1). The axial deformation of the rock high-pressure dynamic test system is measured by a linear variable differential transformer (LVDT), the maximum measurement range is 14 mm, and the deformation loading rate is 0.00001~7 mm/s, the force loading rate is 0.01~300 kN/m, the dynamic load frequency is $0.1 < f < 10$ Hz (load: ±200 kN; dynamic displacement: ±1 mm). The acoustic emission system adopts the Micro-II Express digital acoustic emission detector from American PAC. It has a built-in 18 bit A/D converter and is equipped with 4 high-pass and 6 low-pass filters. The transmission data of acoustic emission waveform data can reach 10 M/s. The update speed of the external parameter input channel is 10 K/s, and the sampling rate is up to 40 MHz. The preamplifier is 20~60 dB.

The acoustic emission sensors were firmly fixed on the coal rock sample surface with elastic band and high vacuum silica gel as the coupling agent (which has the effect of reducing the friction between contact surfaces, reducing the acoustic impedance difference, and reducing the interface energy reflection loss). Two RFAT-30 microsensors are symmetrically arranged at 25 mm at both ends of the sample and in the middle of the sample, and the sensors at three positions are placed in parallel with an angle difference of 45 degrees from top to bottom in the axial direction (see Figure 1). The sampling frequency of the sensors is 150 kHz, it has a good frequency response in the range of 100~450 kHz, and the number of sampling points for each AE signal is 2048. From multiple tests, it can be seen that good test results can be obtained by placing the sensors at three positions in parallel with the axial angle difference of 45° from top to bottom and carrying out 6-channel positioning monitoring. Coal rock specimen size and AE sensors layout as shown in Figure 2(a) and AE sensors three-dimensional localization size as shown in Figure 2(b), positioning size details are shown in Table 1. The pregain of the acoustic emission monitoring system is 45 dB, the threshold value for the triaxial compression test was set to 45 dB, and set the threshold for the dynamic load test to 50 dB for reducing current interference of the testing machine.

3.2. Specimen Preparation. The specimens (samples) were made of the raw coal rock with weak impact-prone from a mine in Binchang mining area (see Figure 3) (including test spare specimen). The dimension of the specimens is diameter × length = 50 mm × 100 mm, the parallelism deviation at both ends of the specimen is less than 0.05 mm, and

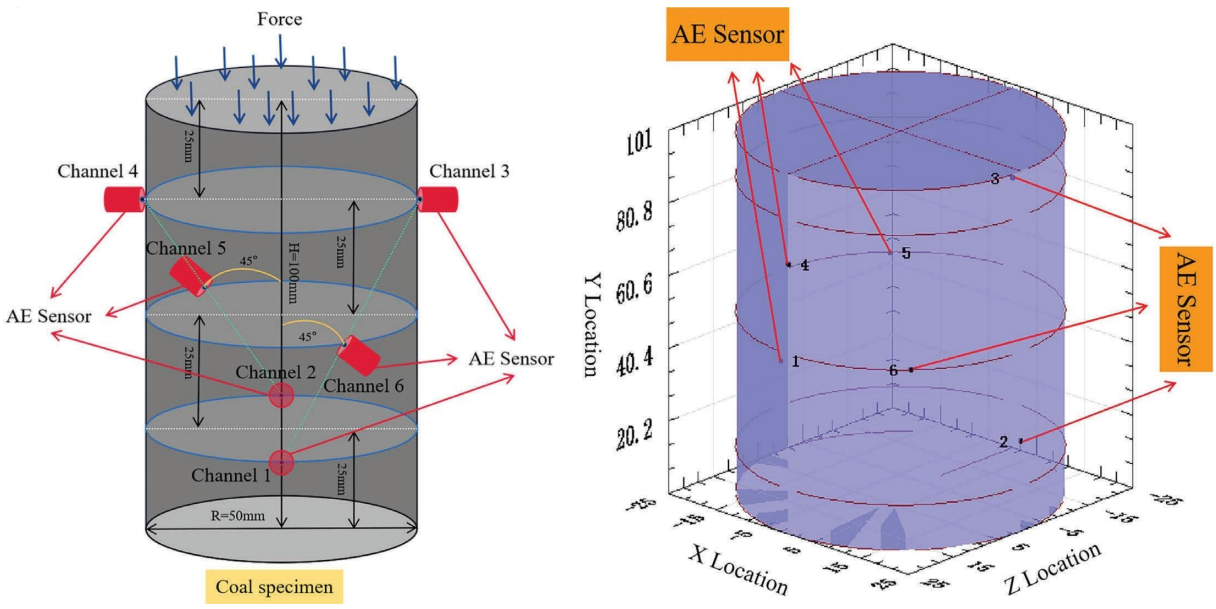

Figure 2: (a) AE coal rock specimen size and the layout of AE sensors; (b) AE sensors localization size display.

Table 1: 3D positioning size table of AE sensors.

Channel	X axis (mm)	Y axis (mm)	Z axis (mm)
1	−25.000	25.000	0.000
2	25.000	25.000	0.000
3	0.000	75.000	−25.000
4	0.000	75.000	25.000
5	−18.000	50.000	−17.000
6	18.000	50.000	17.000

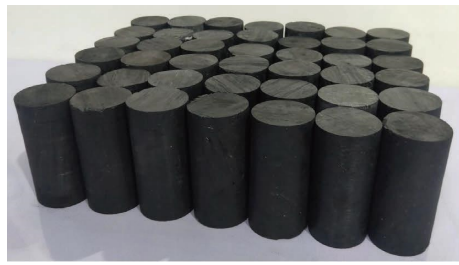

Figure 3: Standard samples.

the perpendicularity deviation of adjacent surfaces is within 0.25°. The samples were screened by lithology, surface characteristics, wave speed measured by a nonmetallic ultrasonic detector, and sample density, and those with high dispersion were removed.

3.3. Engineering Background. When the coal seam is mined, the direct roof above the coal seam forms a cantilevered structure as the empty roof distance in the goaf becomes larger and larger. The self-weight stress of the overlying strata is transferred to the front coal seam to form a high level of supporting stress, so that a large amount of elastic deformation energy is accumulated in the coal seam at the leading part of the working face, the stress concentration is caused by the increase of static load, and the impact risk is also increased. With the advancement of the working face, the overlying strata will break due to the large cantilever distance, and the coal seam at the leading position will suddenly release a large amount of elastic strain energy due to pressure relief. At the same time, after the hard thick roof of the coal seam breaks and falls in the mined-out area. Strong dynamic load will be generated, which will lead to strong rock burst in the working face and surrounding mining area. Specific rock burst induced the process (see Figure 4).

According to the geological survey data of the mine, the mine take the central alleys as tunneling roadway, roadway excavation will not cause large-scale roof caving, and the central alleys as a whole is close to the working face, interval with 200 m coal pillar, after the working face mining, goaf form a large area of empty roof, which in turn caused serious overlying strata roof hanging problem. The roof hanging problem of overlying strata will not only affect the mining face, but also cause high-level supporting stress to the surrounding rock of the adjacent central roadway. Once the roof is fractured, the dynamic load generated will easily induce the dynamic disaster of rock burst in the roadway. The influence mechanism [54] of the roof fracture activity on roadway is shown Figure 5.

The buried depth of coal rock mass at the working face is about 700 m, and the original rock stress of the coal rock is about 12 MPa. The impact load on the coal seam is similar to the seismic wave, the waveform is mostly sine wave, the frequency of the main frequency range is 3~5 Hz, and the duration is usually tens of seconds to several minutes [55]. According to the dynamic load disturbance monitoring near

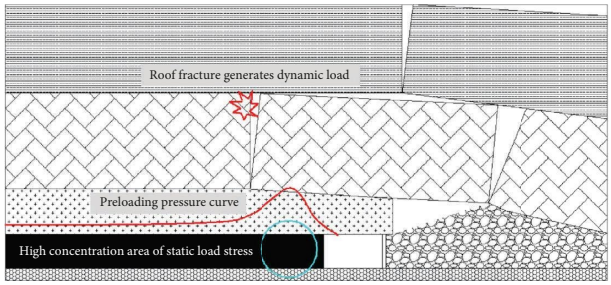

Figure 4: Schematic diagram of rock burst induced by fracture of hard thick roof strata.

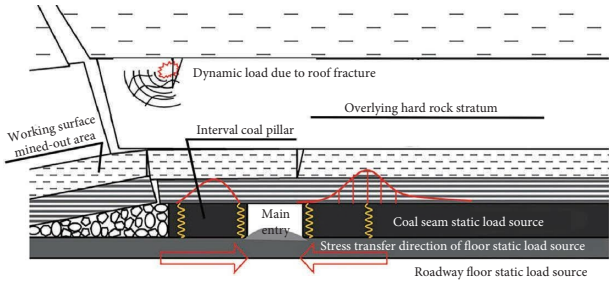

Figure 5: Mechanism of rock burst induced by gob-side roadway.

the working face seismic source, the dynamic load pressure fluctuation is about 5 MPa, and roof pressure distribution of the working face in different periods is shown in Figure 6.

3.4. Test Loading Plan. In order to simulate the mechanical environment of deep-buried impact-prone coal seam under the engineering condition of strong dynamic load caused by the fracture and collapse of hard and thick roof in the goaf, sinusoidal wave load disturbance debugging was carried out by using the Douli test program equipped with the rock high-pressure dynamic test system, and then the sinusoidal wave load acoustic emission failure test was carried out under the confining pressure of 12 MPa, dynamic load frequency of 3, 4, 5, and 6 Hz and amplitude of 10 kN according to the stress characteristics of the original rock suffered by the coal rock mass. During the test, the axial loading rate of 0.01 MPa/s was applied to 12 MPa. And meanwhile, the confining pressure oil pump control system was used to provide pressure for the hydraulic oil in the triaxial pressure chamber. At the loading rate of 0.01 MPa/s, the hydraulic pressure around the sample reached 12 MPa. After the deviatoric stress returned to zero and stabilized, the load was applied on the specimen at an axial deformation rate of 0.001 mm/s until it failed, with the rock high-pressure dynamic test system and the AE monitoring system running synchronously. The test loading plan is presented in Table 2.

4. Analysis of AE *b* Value Characteristics of Coal Rock Failure under Static Loads

During the change of AE *b* value over time, its overall change trend and specific value can not only reflect the stress level inside the coal rock, but also the scale of the derivation, development, and coalescence of cracks in the coal rock. An

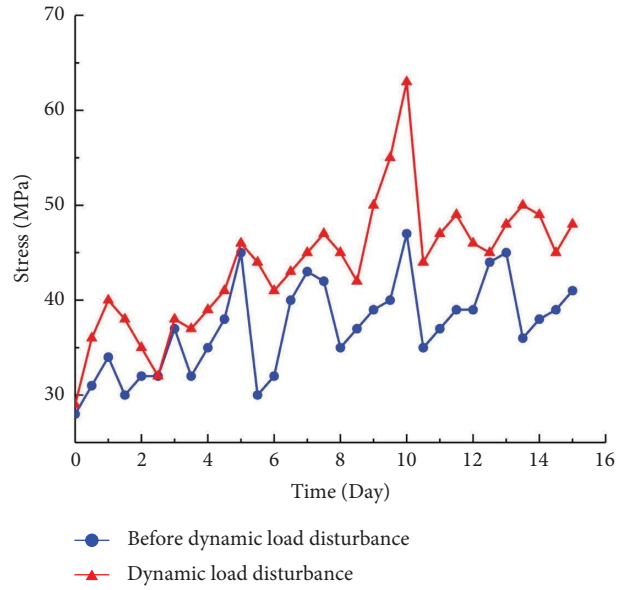

Figure 6: Roof pressure distribution of working face in different periods.

increase in AE *b* value indicates that low-amplitude AE events outstrip high-amplitude ones. When the variation range of *b* value is small and stable, it indicates that the occurrence of high-amplitude and low-amplitude events is relatively stable, that is, the internal cracks in the coal rock have a gradual expansion trend. A dramatic decrease in the *b* value indicates that the cracks grow rapidly, that is, the number of high-amplitude events increases, the stress of coal rock decreases, which may lead to failure of the coal rock.

The drawing data in this paper are obtained from the average value of the parallel test results of each group of samples. Figure 7 shows the variation of stress and acoustic emission *b* value with time in the process of triaxial compression failure of the coal rock.

At the beginning of the experiment, under the confining pressure of 12 MPa, the *b* value of acoustic emission decreases slightly, and the high-amplitude event of acoustic emission accounts for a large proportion. It indicates that a large number of primary cracks, holes, and cracks in the coal rock are compacted and closed to varying degrees under confining pressure stress (I). Then, with the increase of load, coal rock entered the elastic stage (II) in advance, *b* value has been in a high *b* value fluctuation state, the development of the primary crack is stable. As the compressive stress continues to increase into the microfracture stable development stage (III), the microcracks are stable extension and bifurcation, forming microcracks. As the load continues to increase, from the stable development of the crack to the yield stress point, the acoustic emission *b* value shows a slowly increasing trend, and then enters the yield stage (IV), the acoustic emission *b* value decreases sharply, and the microfracture develops rapidly into cracks, and continuously derives new cracks and cracks. The proportion of high energy acoustic emission events increases, and the crack size increases gradually.

Table 2: Design of test plan.

Confining pressure(MPa)	Dynamic load frequency (Hz)	Amplitude (kN)	Loading rate of confining pressure (MPa/s)	Axial loading rate		The number of specimens
				MPa/s	mm/s	
12	0	10	10^{-2}	10^{-2}	10^{-3}	3
	3					5
	4					5
	5					5
	6					5

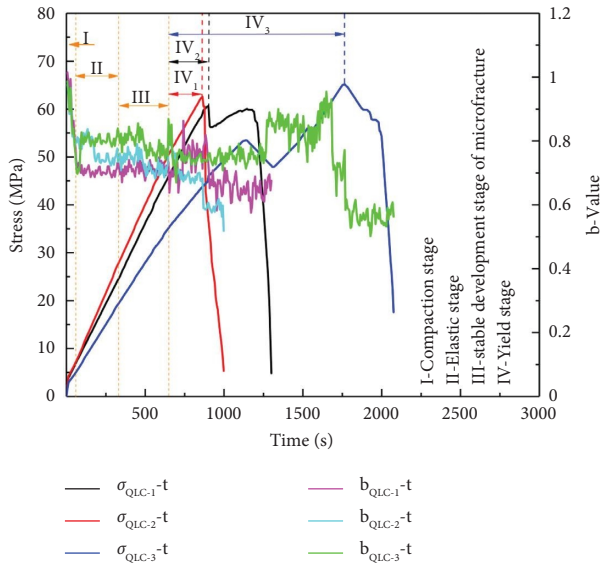

Figure 7: Stress-acoustic emission b value-time relationship of coal rock triaxial compression failure.

Near the end of the yield stage, the b value of acoustic emission shows a sharp decline, and the microcracks and cracks in the coal rock expand rapidly. After reaching the peak stress level, the cracks develop rapidly, cross and assemble to form a penetrating crack, and the coal rock completely loses its bearing capacity. The b value of acoustic emission shows a continuous decline or stable fluctuation trend. The sudden decrease of the acoustic emission b value indicates that the impact-prone coal rock has reached or is about to reach the peak stress level of its structure, indicating that the instability failure will occur.

Due to the strong heterogeneity of the coal rock, shear failure is the dominant mechanism under the action of confining pressure stress [56]. Table 3 lists the triaxial peak axial stress, ultimate strain, and average AE b value of the coal rock specimen.

5. Analysis of Characteristics of AE b Value of Coal Rock Failure under Coupled Static and Dynamic Loads

As a statistical parameter, AE b value reflects the degree to which a region is subjected to average stress and close to the ultimate strength, and it can be used to monitor the disaster incubation of the coal rock resulted from dynamic-load disturbance [57]. As shown in Figure 8, the stress-strain curves of the coal rock at different frequencies present nonlinear characteristics. And the greater the dynamic load frequency, the more obvious the nonlinear characteristics. The slope of the curve loading decreases with the increasing dynamic load frequency. After reaching the yield point, the stress of the coal rock continues to increase to the peak stress with the load. The peak axial stress closest to the average stress of the coal rock under triaxial static load is 62.56 MPa, and the corresponding ultimate strain is 2.655%. At the amplitude of 10 kN, the average peak axial stress is reduced by 8.44%, 13.38%, 20.33%, and 31.97% after loading at 3, 4, 5, and 6 Hz dynamic load frequencies, and the corresponding ultimate strain increases by 10.76%, 19.47%, 25.61%, and 31.47%, respectively.

The results show that the internal cracks and fissures develop rapidly after the coal rock is disturbed by different dynamic load frequencies, so it enters the plastic stage in advance, resulting in brittle failure. And as the dynamic load frequency increases, the process of coal rock failure is accelerated, and the peak strength deterioration and ultimate strain increase become more obvious.

In this paper, the sample whose AE b value is closest to the average AE b value under each dynamic load frequency is selected for analysis. It can be seen from Figure 9 that under the action of confining pressure, the coal rock is in the compaction deformation stage in a short time, and the AE b value decreases slowly or slightly. With the increase of axial load, the original crack expands continuously, and the AE b value is in a stable fluctuation period. After entering the elastic stage and stabilizing, dynamic loads with amplitude of 10 kN and different frequencies have started to be loaded. During the loading process, the AE b value fluctuated in small amplitude or decreased in inclination type (The overall AE b value shows a downward trend of dip angle). And the greater the frequency, the greater the fluctuation amplitude or inclination angle, as shown in Figures 9(a)–9(c).

Under the action of high frequency dynamic load, the friction between coal rock particles is high, the internal microcracks are intensified and evolved, and the high-amplitude events are highly responsive. The coal rock fracture scale increases abruptly, and the AE b value decreases sharply. The dip angle of AE b value decreases with the increase of dynamic load frequency, and the fluctuation amplitude of the AE b value decreases. Compared with the high dynamic load frequency, under the low frequency dynamic load disturbance, the coal rock structure bears the same stress less times in the same time, and the fracture scale

Table 3: Triaxial compression test results of coal rock specimens.

Specimen no	Axial stress σ (MPa)	Axial strain ε (%)	Average AE b value
SLC-1	60.67	3.056	0.705
SLC-2	62.56	2.655	0.725
SLC-3	65.19	3.515	0.757

Description of specimen naming: static load test-coal sample number of static load test..

develops slightly faster with the increase of the disturbance duration. During the dynamic load disturbance process, the low-amplitude events per unit time account for a relatively high proportion, and the internal microcracks extend slowly under the low frequency dynamic load, showing a slow downward trend of AE b value with a larger fluctuation level. In addition, combined with Figures 8 and 9, it can be seen that the dynamic load in the dynamic and static combined loading test is the elastic stage applied to the loading process of the batch of coal rock samples. Under the action of high frequency dynamic load, the AE b value decreases abruptly after a moment of fluctuation. With the increase of dynamic load time, the microcracks and cracks in the coal rock expand rapidly and show irreversible plastic microfracture events. After the end of the dynamic load, a large number of microcracks appear again with the increase of load, and then a certain degree of compaction phenomenon forms a remodeling structure under the strengthening state. Then, under the continuous growth of compressive stress, the microfracture events in the coal rock are stable and developed, resulting in a negative correlation between the dynamic load frequency and the fluctuation of the AE b value. At the same time, it indicates that the dynamic-static combined loading accelerates the evolution process of crack propagation in the impact-prone coal rock, and changes the loading mode of the bearing structure of the system.

In this paper, the decline dip angle of the AE b value is divided into two stages, the first-stage is the dip-type (α_1) downward trend occurring when the dynamic load is disturbed, the second-stage is the dip downward trend (α_2) when the coal rock are about to lose stability and failure. In addition, $0^\circ <$ descent dip angle of the overall numerical value of AE b value $\leq 45^\circ$ is the first-level decrease dip angle, $45^\circ <$ descent dip angle of the overall numerical value of AE b value $<60^\circ$ is the second-level decrease dip angle, $60^\circ <$ descent dip angle of the overall numerical value of AE b value $<90^\circ$ is the third-level decrease dip angle ("cliff jumping type"), 90° descent dip angle of the overall numerical value of AE b value is the fourth-level decrease dip angle ("fault cliff type"). The higher the dynamic load frequency of the coal rock after the dynamic load, the greater the acceleration of AE b value decrease, then the AE b value enters the stable fluctuation period again. Under high frequency (Figure 9(d)) dynamic load, the primary cracks inside the coal rock intensify and expand, and new cracks are derived, the dynamic load disturbance was not over yet, and the AE b value suddenly appeared a "fault cliff type-like" dip angle decrease. Subsequently, the AE b value also entered a stable fluctuation period. After stable fluctuation to peak stress, the AE b value at the four dynamic loading frequencies showed different degrees of "cliff jumping type" and "fault cliff type" decrease. At this time, the pores and cracks inside the coal rock rapidly evolve and expand, showing macroscopic cracks, the bearing capacity of the coal rock decreases and enters the failure stage. As the stress decreases and the strain increases, the AE b value gradually stabilizes until the coal rock is completely destroyed.

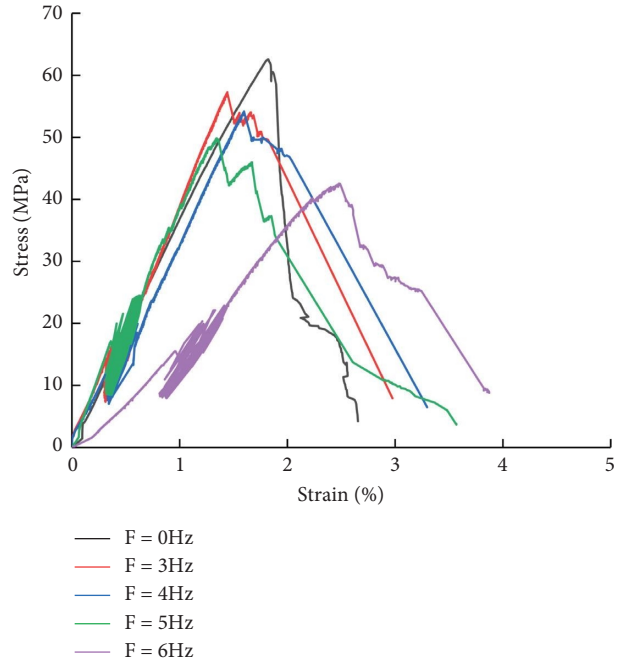

Figure 8: Stress-strain curves of coal rock under coupled static and dynamic loads.

The test results show that with the increase of dynamic load frequency, the time history of the coal rock entering the yield stage is gradually shortened, the bearing level is gradually reduced, and the ultimate strain is gradually increased. At the same time, the higher the dynamic loading frequency, the smaller the average AE b value, and the propagation speed of primary cracks and new cracks in the coal rock is accelerated until the cracks formed through the cracks show macroscopic damage. The AE b value are reduced by 30.32%, 37.04%, 44.17%, and 54.59%, respectively, compared with the average AE b value under triaxial static load. The AE b value during coal rock fracture under increasing frequency dynamic load disturbance, there will be a downward trend of first-stage first-level decrease dip angle, first-stage second-level decrease dip angle, and first-stage "cliff jumping type" decrease dip in turn. While the AE b value shows the rapid decline trend of the second-stage "cliff jumping type" decrease dip angle and the second-stage "fault cliff type" decrease dip angle with the increasing frequency when the coal rock is damaged. This downward trend of the AE b value reflects that the coal rock instability and failure is

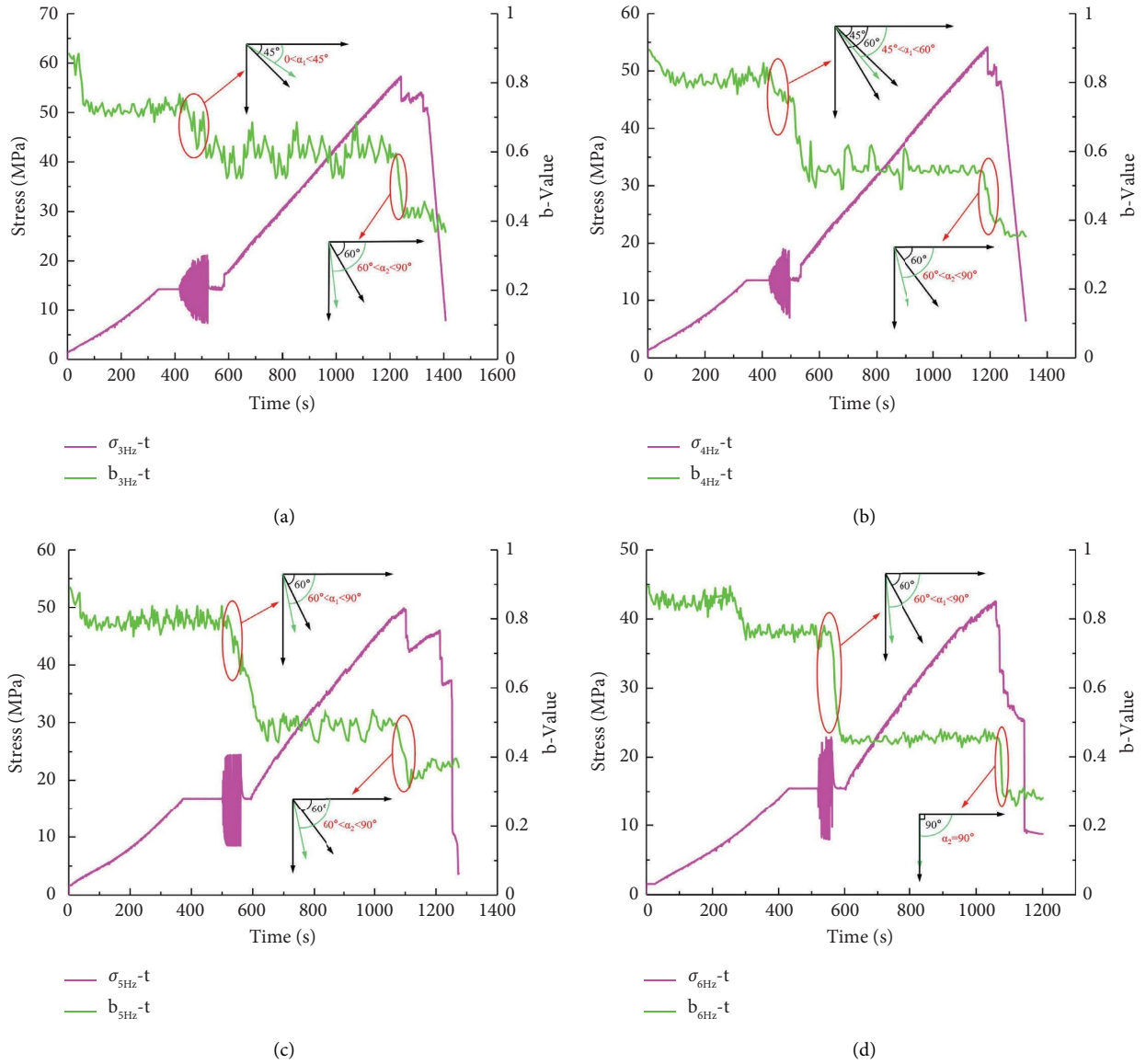

Figure 9: AE *b* value evolution characteristics of coal rock under coupled static and dynamic loads: (a) 3 Hz, (b) 4 Hz, (c) 5 Hz, and (d) 6 Hz.

a process of order reduction. The downward trend of the AE *b* value first-stage decrease dip angle under dynamic load disturbance can be taken as a key opportunity to reveal the potential factors of coal rock destruction and the level of bearing capacity. And then, the accuracy of stability monitoring and early warning of mine coal rock mass engineering is improved.

6. Analysis of AE Signal Parameters Response Characteristics of Coal Rock Failure under Coupled Static and Dynamic Loads

As the loading frequency increases, the overall AE *b* value of coal rock declines, and the AE ringing counts and AE energy generated during the entire instability-failure process change accordingly. The variation trend is presented in Figure 10.

Given that the compaction stage of the coal rock is very short under the action of 12 MPa confining pressure and dynamic load disturbance, so the whole failure process of the coal rock can be divided into the following four stages.

6.1. Compaction and Elastic Stage. The original cracks inside the coal rock are closed and slightly extended and then the coal rock quickly enters the elastic stage under the action of confining pressure. In this case, the coal rock is mainly subjected to elastic deformation and elastic energy accumulates in it. At this stage, due to particle slippage in the coal rock and the closure of original cracks, small-scale microfractures generate, and there are fewer AE events. Even in the stable stage after the slow reduction of the AE *b* value, the AE ringing counts and AE energy are still very small.

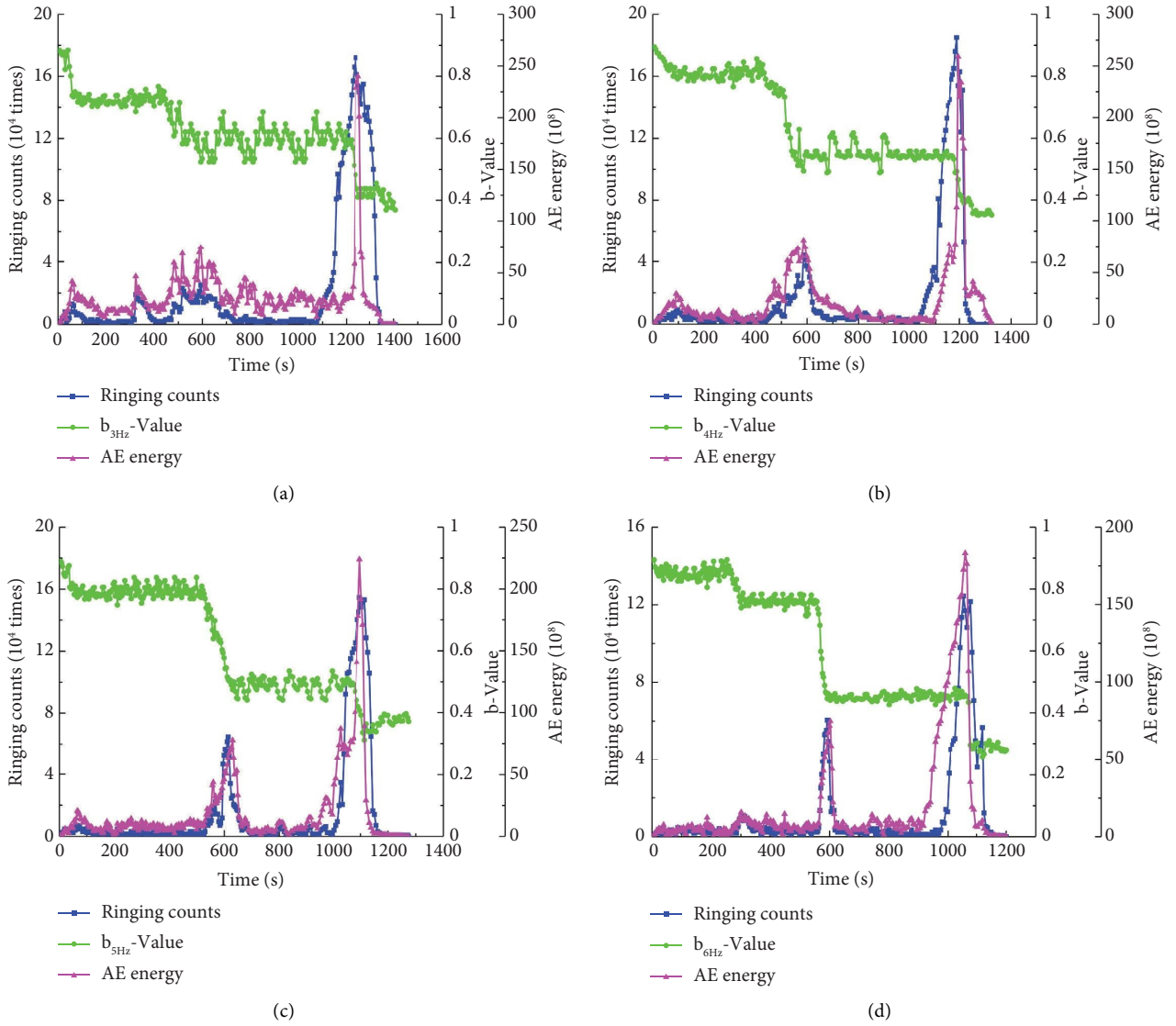

Figure 10: Acoustic emission signal parameters response characteristics under coupled static and dynamic loads of coal rock: (a) 3 Hz, (b) 4 Hz, (c) 5 Hz, and (d) 6 Hz.

6.2. Elastic Acceleration Stage. Under the influence of dynamic load disturbance, small-scale microfractures accelerate and develop, so a large amount of elastic energy is accumulated. The AE *b* value decreases dramatically with the rising frequency, and then it fluctuates steadily again. The AE ringing count and AE energy fluctuate slightly at the initial stage of dynamic load disturbance, and increase significantly after the disturbance ends. After a sharp drop, the AE ringing count and AE energy enters the incubation period. It should be pointed out that in the process of high frequency dynamic load, plastic microfracture has appeared in the coal rock, showing a high amplitude of AE ringing count and AE energy. Under the continuous growth of static load after the end of dynamic load disturbance, part of the plastic microfracture appears to be compacted and closed, and then the closed microfracture and microfracture develop stably under the continuous growth of compressive stress. When the compressive stress increases to the peak stress of the coal rock, the AE ringing count shows the maximum value, and the AE *b* value decreases sharply. When the coal rock structure has a large fracture, the acoustic emission energy value reaches the maximum value. In other words, in the process of dynamic and static combined loading, the higher the dynamic loading frequency, the larger the microfracture scale inside the coal rock, the faster the microfracture development is under the effect of continuous compressive stress growth, and the failure process of the coal rock bearing structure is accelerated. When the compressive stress increases to the peak stress, the fracture degree of the coal rock structure is high. When the coal rock has large fracture, the acoustic emission is abnormally active, but the active degree of the acoustic emission signal is low. Due to the microfracture event under high frequency dynamic load in the elastic stage of the coal rock, the increase of ringing count and acoustic emission energy after 5 Hz and 6 Hz dynamic load disturbance is less than that after 3 Hz and 4 Hz dynamic load disturbance.

The time history of the elastic stage of the coal rock gradually decreases with the increasing dynamic load

frequency. The shortening of the loading time makes the microfractures in the coal rock unable to fully initiate or expand rapidly, so the coal rock quickly enters the plastic stage.

6.3. Plastic Failure Stage. Due to the energy accumulation in the first two stages, coal rock appears to be partially damaged and its bearing capacity is reduced. The cracks inside the coal rock develop into fissures, which continue to grow with the newly-generated cracks. The fluctuation range of the AE b value increases slightly, while the AE ringing count and AE energy produced by the coal rock show a sharp increase.

6.4. Instability and Failure Stage. In this stage, the microcracks in the coal rock develop into large-scale cracks, and the intersection and penetration of the large cracks lead to instability and failure of the coal rock. After reaching the peak stress, the decreasing amplitude of the AE b value increases with the increasing dynamic load frequency, and the AE ringing count and AE energy also reach the peak. As shown in Figure 10, the ringing count and AE energy peak after dynamic load disturbance of frequency 5 Hz and 6 Hz (Figures 10(c) and 10(d)) are lower than those after dynamic load disturbance of 3 Hz and 4 Hz (Figures 10(a) and 10(b)). The change trends of AE ringing count and AE energy of the coal rock with weak outburst-proneness after high frequency dynamic load disturbance are similar to the AE response characteristics of the coal rock with strong impact tendency, that is, the overall AE ringing count and AE energy of the strong impact tendency coal rock are much smaller than those of the weak impact-prone coal rock [58]. The test results show that weak impact-prone coal rock tends to evolve towards the strong impact tendency coal rock as the dynamic load disturbance frequency increases.

7. Conclusions

Through analyzing the triaxial acoustic emission test results of the coal rock, this paper studies the variation law of the AE b value of the coal rock before and after dynamic load disturbance and that under different dynamic load frequencies, and obtains the evolution characteristics leading to instability and failure of the coal rock. The major conclusions drawn are as follows:

(1) The increase in dynamic loading frequency will accelerate the instability/failure process of the impact-prone coal rock. As the dynamic load frequency increases, the average stress of the coal rock decreases, while the ultimate strain increases. Compared with the static load, the average stress is reduced by about 1/3 at the maximum, and the ultimate strain is increased by about 1/3 at the most.

(2) Under the disturbance of dynamic load, the proportion of high-amplitude events is relatively high. This means that the overall AE b value is lower than that under static load. Moreover, the higher the dynamic load frequency, the greater the decrease in the AE b value. The first-stage dip angle decrease of the acoustic emission b value can be used as early warning information of impact-prone coal rock failure precursor, while the occurrence of the second-stage "cliff jumping type" decrease dip angle and the second-stage "fault cliff type" decrease dip angle indicates that the coal rock is about to lose stability and failure.

(3) With the increase of dynamic load frequency, the AE ringing count and AE energy after dynamic load disturbance first increase and then decrease, and they have a significant negative correlation with the AE b value before and after the dynamic loading (till the coal rock fails).

(4) The AE response characteristics of the weak impact-prone coal rock under the action of dynamic load disturbance gradually evolve to the AE response characteristics of the strong one as the frequency of dynamic loads increases.

Data Availability

The datasets used in the present study are available from the corresponding author upon reasonable request.

Conflicts of Interest

The authors declare that they have no conflicts of interest.

Acknowledgments

The research was supported by the National Natural Science Foundation of China (No. 12072259) and Coal Joint Fund of Shaanxi Natural Science Foundation of China (No. 2019JLP-01).

References

[1] H. P. Xie, F. Gao, and Y. Ju, "Novel idea and disruptive technologies for the exploration and research of deep earth," *Advanced Engineering Sciences*, vol. 49, no. 1, pp. 1–8, 2017.

[2] J. P. Tang, N. Hao, Y. S. Pan, and S. J. Sun, "Experimental study on precursor characteristics of coal and gas outbursts based on acoustic emission energy analysis," *Chinese Journal of Rock Mechanics and Engineering*, vol. 40, no. 1, pp. 31–42, 2020.

[3] X. L. Li, Z. H. Li, E. Y. Wang et al., "Microseismic signal spectra, energy characteristics, and fractal features prior to rock burst: a case study from the qianqiu coal mine, China," *Journal of Earthquake Engineering*, vol. 21, no. 6, pp. 891–911, 2017.

[4] Y. D. Jiang, Y. S. Pan, F. X. Jiang, L. M. Dou, and Y. Ju, "State of the art review on mechanism and prevention of coal bumps in China," *Journal of China Coal Society*, vol. 39, no. 2, pp. 205–213, 2014.

[5] Q. X. Qi, Y. S. Pan, and H. T. Li, "Theoretical basis and key technology of prevention and control of coal-rock dynamic disasters in deep coal mining," *Journal of China Coal Society*, vol. 45, no. 5, pp. 17–34, 2020.

[6] Z. Yu, J. Wen, Q. Zhu, H. Ma, and Y. Feng, "A combined denoising method for microseismic signals from coal seam

hydraulic fracturing: multithreshold wavelet packet transform and improved hilbert-huang transform," *Shock and Vibration*, vol. 2021, no. 3, Article ID 6623861, 15 pages, 2021.

[7] Z. L. Wu, "Progress and prospect of AE signal parameters in prediction of coal (rock) and gas outburst risk," *Mining Safety and Environmental Protection*, vol. 1, pp. 27–29, 2005.

[8] Q. Zhang and X. P. Zhang, "A numerical study on cracking processes in limestone by the b-value analysis of acoustic emissions," *Computers and Geotechnics*, vol. 92, pp. 1–10, 2017.

[9] S. M. Liu, X. L. Li, D. K. Wang, and D. Zhang, "Investigations on the mechanism of the microstructural evolution of different coal ranks under liquid nitrogen cold soaking," *Energy Sources, Part A: Recovery, Utilization, and Environmental Effects*, no. 7, pp. 1–17, 2020.

[10] M. Cai, H. Morioka, P. K. Kaiser et al., "Back-analysis of rock mass strength parameters using AE monitoring data," *International Journal of Rock Mechanics and Mining Sciences*, vol. 44, no. 4, pp. 538–549, 2007.

[11] Q. Lou, D. Z. Song, X. Q. He et al., "Correlations between acoustic and electromagnetic emissions and stress drop induced by burst-prone coal and rock fracture," *Safety Science*, vol. 115, no. 6, pp. 310–319, 2019.

[12] J. Manterloa, M. Aguirre, and J. Zurbitu, "Using acoustic emissions (AE) to monitor mode I crack growth in bonded joints," *Engineering Fracture Mechanics*, vol. 2241, no. 2, Article ID 106778, 2020.

[13] R. Jiang, F. Dai, Y. Liu, A. Li, and P. Feng, "Frequency characteristics of acoustic emissions induced by crack propagation in rock tensile fracture," *Rock Mechanics and Rock Engineering*, vol. 54, no. 4, pp. 2053–2065, 2021.

[14] X. X. Liu, Z. Z. Liang, Y. B. Zhang, P. Liang, and B. Tian, "Experimental study on the monitoring of rockburst in tunnels under dry and saturated conditions using AE and infrared monitoring," *Tunnelling and Underground Space Technology*, vol. 82, no. 12, pp. 517–528, 2018.

[15] A. Schiavi, G. Lacidogna, and G. Niccolini, "Analysis of acoustic emissions at low frequencies in brittle materials under compression," in *Proceedings of the SEM Annual Conference Albuquerque New Mexico USA Society for Experimental Mechanics Inc*, Albuquerque, NM, USA, June 2009.

[16] X. L. Li, S. J. Chen, S. M. Liu, and Z. H. Li, "AE waveform characteristics of rock mass under uniaxial loading based on Hilbert-Huang transform," *Journal of Central South University*, vol. 28, no. 6, pp. 1843–1856, 2021.

[17] V. L. Shkuratnik, Y. L. Filimonov, and S. V. Kuchurin, "Regularities of acoustic emission in coal samples under triaxial compression," *Journal of Mining Science*, vol. 41, no. 1, pp. 44–52, 2005.

[18] Y. Liu, F. Dai, L. Dong, N. W. Xu, and P. Feng, "Experimental investigation on the fatigue mechanical properties of intermittently jointed rock models under cyclic uniaxial compression with different loading parameters," *Rock Mechanics and Rock Engineering*, vol. 51, no. 1, pp. 47–68, 2018.

[19] J. J. Feng, E. Y. Wang, Q. S. Huang, H. Ding, and Y. Ma, "Study on coal fractography under dynamic impact loading based on multifractal method," *Fractals*, vol. 28, no. 1, Article ID 2050006, 2020.

[20] X. P. Lai, H. C. Xu, J. D. Fan et al., "Study on the mechanism and control of rock burst of coal pillar under complex conditions," *Geofluids*, vol. 2020, no. 2, Article ID 8847003, 19 pages, 2020.

[21] X. Li, S. Chen, E. Wang, and Z. Li, "Rockburst mechanism in coal rock with structural surface and the microseismic (MS) and electromagnetic radiation (EMR) response," *Engineering Failure Analysis*, vol. 124, no. 6, Article ID 105396, 2021.

[22] X. G. Kong, S. G. Li, E. Y. Wang et al., "Dynamics behaviour of gas-bearing coal subjected to SHPB tests," *Composite Structures*, vol. 256, Article ID 113088, 2021.

[23] X. P. Lai, X. W. Fang, F. Cui, and P. F. Shan, "Damage evolution of coal and rock under impact load," *Journal of Xi'an University of Science and Technology*, vol. 39, no. 6, pp. 919–927, 2019.

[24] F. Dai, Y. Xu, T. Zhao, N. W. Xu, and Y. Liu, "Loading-rate-dependent progressive fracturing of cracked chevron-notched Brazilian disc specimens in split Hopkinson pressure bar tests," *International Journal of Rock Mechanics and Mining Sciences*, vol. 88, pp. 49–60, 2016.

[25] H. Sun, X. L. Liu, and Y. L. Chen, "Experimental on coupling properties of stress and acoustic emission during coal and rock fracture under multilevel dynamic loadings," *Chinese Journal of Rock Mechanics and Engineering*, vol. 37, pp. 279–288, 2018.

[26] Z. L. Zhou, X. Cai, X. B. Li, W. Z. Cao, and X. M. Du, "Dynamic response and energy evolution of sandstone under coupled static–dynamic compression: insights from experimental study into deep rock engineering applications," *Rock Mechanics and Rock Engineering*, vol. 53, no. 3, pp. 1305–1331, 2020.

[27] Y. Xu, F. Dai, and H. B. Du, "Experimental and numerical studies on compression-shear behaviors of brittle rocks subjected to combined static-dynamic loading," *International Journal of Mechanical Sciences*, vol. 175, Article ID 105520, 2020.

[28] Z. L. Yan, F. Dai, Y. Liu, H. Du, and J. Luo, "Dynamic strength and cracking behaviors of single-flawed rock subjected to coupled static–dynamic compression," *Rock Mechanics and Rock Engineering*, vol. 53, no. 9, pp. 4289–4298, 2020.

[29] Z. L. Yan, F. Dai, J. B. Zhu, and Y. Xu, "Dynamic cracking behaviors and energy evolution of multi-flawed rocks under static pre-compression," *Rock Mechanics and Rock Engineering*, vol. 54, no. 9, pp. 5117–5139, 2021.

[30] X. Li, Z. Zhou, T. S. Lok, L. Hong, and T. Yin, "Innovative testing technique of rock subjected to coupled static and dynamic loads," *International Journal of Rock Mechanics and Mining Sciences*, vol. 45, no. 5, pp. 739–748, 2008.

[31] L. Weng, X. B. Li, A. Taheri, Q. H. Wu, and X. F. Xie, "Fracture evolution around a cavity in brittle rock under uniaxial compression and coupled static-dynamic loads," *Rock Mechanics and Rock Engineering*, vol. 51, no. 2, pp. 531–545, 2018.

[32] D. Li, F. Gao, Z. Han, and Q. Zhu, "Experimental evaluation on rock failure mechanism with combined flaws in a connected geometry under coupled static-dynamic loads," *Soil Dynamics and Earthquake Engineering*, vol. 132, Article ID 106088, 2020.

[33] F. J. Yang, D. W. Hu, and H. Zhou, "Physical and mechanical properties of granite after dynamic disturbance," *Chinese Journal of Rock Mechanics and Engineering*, vol. 37, no. 6, pp. 1459–1467, 2018.

[34] F. J. Zhao, H. Y. Wang, and Y. Peng, "Experimental research on acoustic emission energy and rock crushing effect under combined static-dynamic coupling loading," *Chinese Journal of Rock Mechanics and Engineering*, vol. 31, no. 7, pp. 77–82, 2012.

[35] L. M. Zhang, S. Q. Ma, and M. Y. Ren, "Acoustic emission frequency and b value characteristics of rock failure process

under various confining pressures," *Chinese Journal of Rock Mechanics and Engineering*, vol. 34, no. 10, pp. 2057–2063, 2015.

[36] K. Mogi, "Effect of the intermediate principal stress on rock failure," *Journal of Geophysical Research*, vol. 72, no. 20, pp. 5117–5131, 1967.

[37] X. Lei, "How do asperities fracture? An experimental study of unbroken asperities," *Earth and Planetary Science Letters*, vol. 213, no. 3-4, pp. 347–359, 2003.

[38] J. H. Tang, X. D. Chen, F. Dai, and M. D. Wei, "Experimental investigation of fracture damage of notched granite beams under cyclic loading using DIC and AE techniques," *Fatigue and Fracture of Engineering Materials and Structures*, vol. 43, no. 7, pp. 1583–1596, 2020.

[39] X. L. Liu, M. C. Pan, X. B. Li, and J. P. Wang, "Acoustic emission b-value characteristics of granite under dynamic loading and static loading," *Chinese Journal of Rock Mechanics and Engineering*, vol. 36, no. 332, pp. 35–42, 2017.

[40] R. V. Sagar, B. R. Prasad, and S. S. Kumar, "An experimental study on cracking evolution in concrete and cement mortar by the b-value analysis of acoustic emission technique," *Cement and Concrete Research*, vol. 42, no. 8, pp. 1094–1104, 2012.

[41] L. Calabrese, E. Proverbio, D. Di Pietro, A. Donato, and M. Galeano, "The use of b-value and Ib-value of acoustic emission in monitoring hydrogen-assisted cracking of martensitic stainless steel," *International Journal of Microstructure and Materials Properties*, vol. 12, no. 3/4, pp. 165–182, 2017.

[42] T. H. W Goebel, D. Schorlemmer, T. W. Becker, G. Dresen, and C. G. Sammis, "Acoustic emissions document stress changes over many seismic cycles in stick slip experiments," *Geophysical Research Letters*, vol. 40, no. 10, pp. 2049–2054, 2013.

[43] Y. Niu, X. P. Zhou, and L. S. Zhou, "Fracture damage prediction in fissured red sandstone under uniaxial compression: acoustic emission b value analysis," *Fatigue and Fracture of Engineering Materials and Structures*, vol. 43, no. 1, pp. 175–190, 2020.

[44] L. J. Dong, L. Y. Zhang, H. N. Liu, K. Du, and X. L. Liu, "Acoustic emission b value characteristics of granite under true triaxial stress," *Mathematics*, vol. 10, no. 3, pp. 451–467, 2022.

[45] X. L. Li, S. J. Chen, S. Wang, M. Zhao, and H. Liu, "Study on in situ stress distribution law of the deep mine taking Linyi Mining area as an example," *Advances in Materials Science and Engineering*, vol. 2021 Article ID 5594181, 11 pages, 2021.

[46] X. L. Li, Z. Y. Cao, and Y. L. Xu, "Characteristics and trends of coal mine safety development," *Energy Sources, Part A: Recovery, Utilization, and Environmental Effects*, pp. 1–19, 2020.

[47] H. Y. Liu, B. Y. Zhang, X. L. Li et al., "Research on roof damage mechanism and control technology of gob-side entry retaining under close distance gob," *Engineering Failure Analysis*, vol. 138, Article ID 106331, 2022.

[48] S. H. Liu, F. M. Li, H. Lan, J. F. Pan, and T. T. Du, "Experimental study on failure characteristics and mechanism of coal under coupled static and dynamic loads," *Chinese Journal of Rock Mechanics and Engineering*, vol. 32, no. S2, pp. 3749–3759, 2013.

[49] Z. W. Zeng, J. Ma, L. Q. Liu, and T. C. Liu, "Dynamic characteristics and significance of acoustic emission b-value during rock fracture propagation," *Seismogeology*, vol. 17, no. 1, pp. 7–12, 1995.

[50] B. Gutenberg and C. F. Richter, "Frequency of earthquakes in California," *Bulletin of the Seismological Society of America*, vol. 34, no. 4, pp. 185–188, 1944.

[51] J. J. Zhao, Q. Fan, and P. F. Li, "Acoustic emission b value characteristics and failure precursor of the dacite under different stress paths," *Journal of Engineering Geology*, vol. 27, no. 3, pp. 487–496, 2019.

[52] W. F. Sun and H. D. Gu, "How to correctly calculate b-value," *Journal of Disaster Prevention and Mitigation*, vol. 4, pp. 13–27, 1992.

[53] F. Sagasta, M. E. Zitto, R. Piotrkowski, A. Benavent-Climent, E. Suarez, and A. Gallego, "Acoustic emission energy b-value for local damage evaluation in reinforced concrete structures subjected to seismic loadings," *Mechanical Systems and Signal Processing*, vol. 102, no. 1, pp. 262–277, 2018.

[54] J. F. Pan, S. H. Liu, and J. M. Gao, "Prevention theory and technology of rock burst with distinguish dynamic and static load sources in deep mine roadway," *Journal of China Coal Society*, vol. 45, no. 5, pp. 1607–1613, 2020.

[55] J. X. Ren, S. Jing, and K. Zhang, "Study on failure mechanism and acoustic emission characteristics of outburst proneness coal under dynamic and static loading," *Coal Science and Technology*, vol. 49, no. 3, pp. 57–63, 2021.

[56] J. P. Zuo, H. P. Xie, A. M. Wu, and J. F. Liu, "Investigation on failure mechanisms and mechanical behaviors of deep coal-rock single body and combined body," *Chinese Journal of Rock Mechanics and Engineering*, vol. 30, no. 1, pp. 84–92, 2011.

[57] Q. L. Li, J. T. Chen, L. Yu, and B. L. Hao, "b-value spatio-temporal scanning-a means of monitoring the process of destructive earthquakes," *Acta Geophysica Sinica*, vol. 2, pp. 101–125, 1978.

[58] H. Y. Li, L. J. Kang, Z. J. Xu, Q. X. Qi, and S. K. Zhao, "Precursor information analysis on acoustic emission of coal with different outburst proneness," *Journal of China Coal Society*, vol. 39, no. 2, pp. 384–388, 2014.